Autonomous Attitude Control System for the Ørsted Satellite

Søren Abildsten Bøgh, Rafał Wiśniewski, and Thomas Bak

Aalborg University, Department of Control Engineering,
Frederik Bajers Vej 7, DK-9220 Aalborg Ø, Denmark.
email: {sbg,raf,tb}@control.auc.dk

Abstract: Attitude control for small satellites differ from traditional attitude control systems by having simple hardware and inexpensive actuators imposed by cost constraints. Limited ground contact, on the other hand, imposes requirements to autonomy of the attitude control. These conflicting requirements are fulfilled through development of novel attitude and control algorithms combined with an on-board supervisory control architecture.
Attitude estimation with an extended Kalman filter using sun sensor and magnetometer data is introduced as a backup to a star camera estimate. This enables continued operation in case of star camera or sun sensor failures. Three-axis attitude stabilization is provided with use of a set of three perpendicular magnetorquers. The attitude control and estimation algorithms are integrated into a supervisory control architecture that enables reconfiguration in real time, based on mission phase and contingency operation requirements. This provides some level of fault tolerance with graceful degradation in case of severe faults.
Results from simulations are presented to demonstrate projected performance capability.

Keywords: Small satellites, attitude determination and control, extended Kalman filter, magnetic control, periodic systems, fault detection, reconfiguration, autonomy, supervisory control.

1. INTRODUCTION

Small satellites represent a new area where traditional approaches to attitude control often cannot be applied. Short development time and modest budgets limits the available solutions. One possible solution is to avoid dedicated sensors for attitude control and rely on science instruments for attitude acquisition. Low pointing requirements could be utilized in the selection of simple actuators.

The Danish Ørsted satellite is an advanced small scientific satellite with a high quality science payload. The attitude control subsystem on Ørsted has been based on input from the science instruments in the extent possible combined with a simple magnetic control principle.

The Ørsted satellite is controlled from only one ground station situated in Denmark permitting only 2-3 contact periods of 10 minutes each day. Therefore, autonomous operation and on-board fault handling is required to avoid serious impact on the scientific mission or even loss of the satellite. Some of the functionality that is traditionally implemented on ground stations must, consequently, be moved to the space segment.

The Ørsted attitude estimation is primarily based on the science star camera, but a gyro-less backup algorithm based on sun sensors and magnetometer data is outlined in the paper. The backup algorithm produces attitude estimates even in eclipse conditions and in case of sun sensor failures, providing a significant level of autonomy.

The attitude controller provides active detumbling and three-axis stabilization of the satellite using solely three perpendicular magnetorquers. If the boom is detected to be upside-down the attitude is acquired employing an inverted boom controller.

This paper also contributes with a new approach in development of supervisory control in a systematic manner. A general strategy is proposed that seeks to improve the performance of reconfigurable control systems. Previous missions with focus on similar aspects of autonomy are Ulysses [1], Clementine [2], and the XTE spacecraft [3]. The concept of autonomy is, anyhow, accepted differently with various levels of automation. Future missions include NASA's New Millennium Programme [4] and the Japanese MUSES-C satellite [5].

The paper first gives an introduction to the satellite equipment with a description of the environment in which the ACS operates. The structure of the ACS is then presented, which highlights the three main modules of ACS: 1) attitude control, 2) attitude determination, and 3) supervisory control. These are treated individually in the paper with simulation results in each section. The section about supervisory control combines determination and control and gives an example on the necessity of fault detection and reconfiguration.

2. THE ØRSTED SATELLITE

Ørsted is scheduled for launch in Autumn 1997 from Vandenberg, California. The science mission is related to the geomagnetic field and its interaction with the solar wind plasma. It is launched into a 450 $\times$ 850 km orbit with a 96 degree inclination by a Delta II launcher. After release ACS captures the satellite from a random tumbling and an 8 meter boom is deployed. In the remaining part of the mission the ACS is required to stabilize the satellite in three axes with the boom pointing away from the Earth, see Figure 1.

The science instruments are located on platforms displaced from the main body to minimize EMC interference. The magnetic field vector is measured with an accuracy of 1.5 nT using a three-axis Compact Spherical Coil (CSC) fluxgate magnetometer [6]. Magnetic calibration is performed in-flight using a scalar magnetometer with an absolute measurement error less than 0.5 nT. A CCD based star camera provides inertial attitude estimates with a bore axis accuracy of 2 arcsec and angular resolution around the bore axis of 10 arc seconds [7]. The star camera operation is constrained by bright objects in the field of view, and a maximum angular velocity of 10 deg/min. On the main body six solid state charged particle detectors measure high energy electrons, protons, and Alpha particles. Two GPS receivers (TANS from Trimble Navigation and TurboRogue from JPL) provide position estimates better than $\pm$50 m, velocity within $\pm$0.5 m/sec, and UTC time within 1 microsec.

On the main body eight sets of two-redundant sun sensors provide a near 4π steradian field of view with an accuracy on the sun incident angle determination of 4 deg. Control actuation is provided by three perpendicular two-

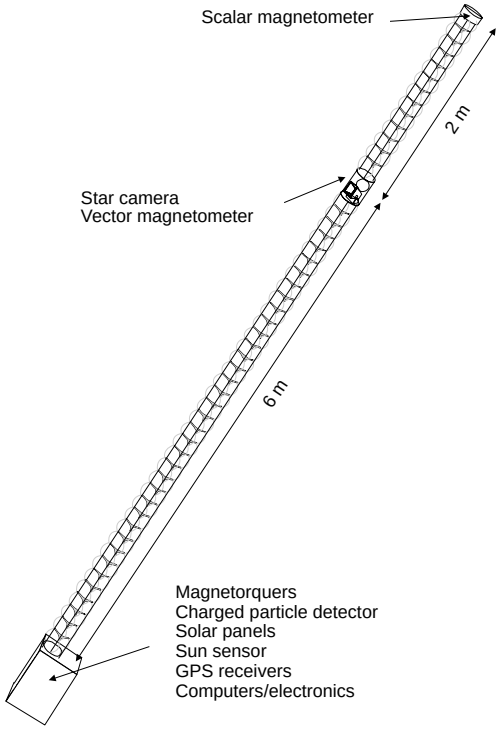

Figure 1: *The Ørsted satellite in the boom deployed configuration.*

redundant air-cored magnetorquers with a peak torque of 10^{-3} Nm.

The requirements to the ACS are derived from power optimization as well as the field of view and rate sensitivity of the star camera. Attitude is required below 10 deg in pitch/roll and 20 deg in yaw. The angular velocity shall be below 10 deg/min. The pointing requirements translates into requirements to the on-board attitude knowledge. The pitch/roll requirement is 2 deg. The yaw requirement is 4 deg. The error in rate estimates should be below 0.01 deg/min.

The ACS software is integrated with the on-board data handling software on an Intel 80186, 16 MHz computer platform. The software is developed using Ada language which provides real-time multitasking.

3. ATTITUDE CONTROL SYSTEM ARCHITECTURE

The Ørsted ACS is responsible for multiple tasks: execution of the fundamental control and estimation, validation of sensor outputs, handling of hardware faults, management of operational commands and monitoring information. To facilitate these functions a systematic approach has been taken resulting in a the three level structure shown in Figure 2.

The assignments of the 3 levels are

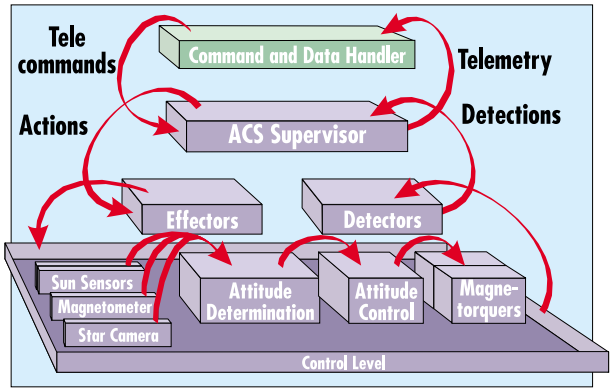

Figure 2: *ACS structure with a supervisor for fault handling and telecommand/telemetry interface.*

- A lower level with input/output and the fundamental control loop.
- A second level with algorithms for fault detection and fault accommodation.
- A third level with supervisor logic and communication with the satellite command and data handler.

The control level is the feedback loop with sensor processing, attitude acquisition/control, and actuation. It is designed and tested in each individual mode that is specified by different operational phases and sensor configurations. The supervisor design guarantees selection of the correct mode in different situations.

The detectors are signal processing units that observe the system and compares with the expected system behaviour. An alarm is raised when an anomaly is detected. The Effectors execute the remedy actions associated with fault accommodation.

The supervisor reacts on the current condition, receiving inputs from detectors and commands from the satellite command distributor. From a set of logical rules, the supervisor determines the appropriate actions to be executed on the control level and the telemetry to be generated.

4. ATTITUDE CONTROL

Stabilization of the Ørsted satellite is accomplished by active use of a set of mutually perpendicular coils, magnetorquers. The interaction between the external magnetic field of the Earth and the magnetic field generated in the coils produces a mechanical torque, which is used to correct the attitude. The satellite actuated by a set of magnetorquers has a serious limitation. The mechanical torque produced by the coils is always perpendicular to the geomagnetic field vector. Thus, the direction parallel to the geomagnetic field vector is not controllable. The geomagnetic field changes its orientation when the satellite moves on orbit. This implies that yaw is not controllable in the polar regions and roll is not controllable in the equatorial regions.

Dependent on the operational mode three separate attitude controllers have been developed: 1) the rate detumbling controller, 2) the science observation controller, and 3) the inverted boom controller.

4.1. Rate Detumbling Control

The objective of the rate detumbling controller is to generate a magnetic moment, such that the kinetic energy of the satellite is dissipated and it is turned in the direction of the local geomagnetic field vector. This will cause the satellite antennas to point towards the Earth above Denmark.

Hence, the deployment of the scientific boom in polar regions is viable. The influence of the gravity gradient on the satellite in a boom stowed configuration is negligible.

The kinetic energy, E_k, of the rotary motion is:

$$E_k = \frac{1}{2}\boldsymbol{\Omega}_{cw}^T \, \mathbf{I} \, \boldsymbol{\Omega}_{cw}, \tag{1}$$

where $\boldsymbol{\Omega}_{cw}$ is the satellite angular velocity with respect to an inertial coordinate system, and $\mathbf{I}$ is the inertia tensor.

Lyapunov theory has been applied in [8] to prove that E_k is dissipated with the following control law:

$$\mathbf{m} = -k \, \dot{\mathbf{B}}, \tag{2}$$

where $\mathbf{m}$ is the magnetic moment, $\mathbf{B}$ is the local geomagnetic field vector, and k is a positive constant (control gain).

This controller does not ensure directional control, however. To force the z-principal axis of the satellite to track the inverse direction of the geomagnetic field a constant term is added to the control law in Eq. (2):

$$\mathbf{m} = -k \, \dot{\mathbf{B}} - \mathbf{m}_{const}, \tag{3}$$

where $\mathbf{m}_{const} = [0 \; 0 \; m_{const}]^T$. Now the satellite acts like a compass needle which tends to align with the local geomagnetic field, while adequate angular velocity damping is retained.

The algorithm for the rate detumbling controller has been verified by simulations. Figure 3 shows simulation results for the worst case initial value of the satellite angular velocity $\boldsymbol{\Omega}_{cw}(t_0) = [0.10 \; 0.10 \; 0.09]^T$ rad/s.

The first plot depicts the satellite inertial angular velocity. Already after the first orbit the angular velocity is decreased to $[0.0006 \; 0.0033 \; 0.0001]^T$ rad/s. The velocity does not diminish to zero, since the rate of the geomagnetic field is nonzero in the inertial coordinate system. The second plot shows the time history of satellite

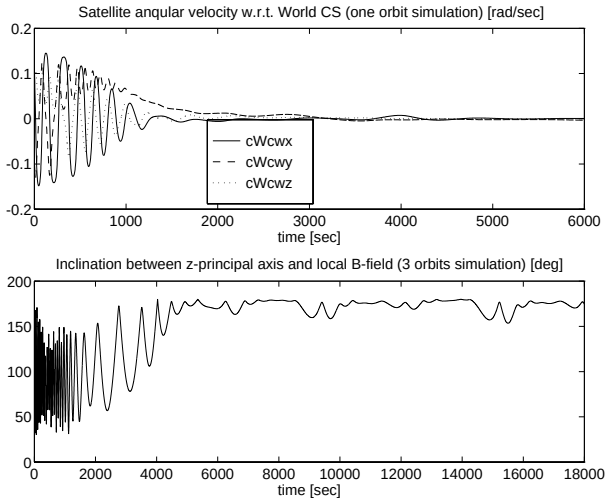

Figure 3: *Rate detumbling simulation. Satellite tracks the inverse geomagnetic field vector*.

attitude. The satellite tracks the inverse direction of the geomagnetic field. The rate of the geomagnetic field is largest in the equatorial regions giving difficulties for the satellite to track the field vector. This phenomena causes the periodic peaks of the inclination angle.

Figure 4 shows the deviation of the boom axis from zenith for one orbit. The deviation is below 20 deg at 56 deg North, which is the latitude of Denmark. It is concluded that the radio contact with the Danish ground station can be established.

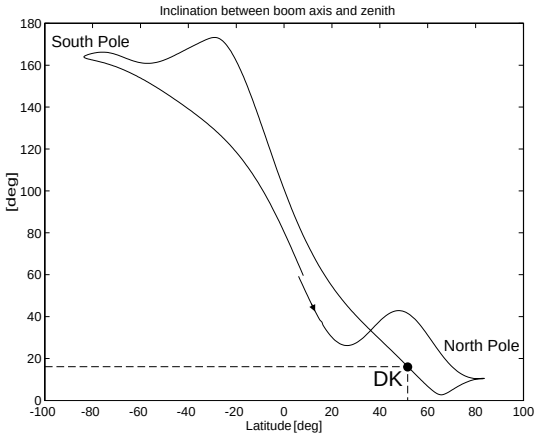

Figure 4: *Rate detumbling simulation. The plot shows the steady state deviation of the boom axis from zenith for one orbit. The deviation is below 20 deg at 56 deg North, which is the latitude of Denmark.*.

4.2. Science Observation Control

The aim of the science observation control is to provide three-axis stabilization of the satellite after boom deployment. Design of the science observation controller is based on a linear approach since the satellite trajectory remains in a neighbourhood of a reference, due to the influence of the conservative forces of the gravity gradient and the gyro-effect caused by the rotation of the satellite around the Earth.

The observation that the geomagnetic field in a near polar orbit is approximately periodic with period $T_o = 2\pi/\omega_o$ (ω_o is the orbital rate) can be used in the design of a constant gain controller.

The linearized equations of motion are symbolically given by (for more details see [9]):

$$\frac{d}{dt}\begin{bmatrix} \delta\mathbf{\Omega} \\ \delta\mathbf{q} \end{bmatrix} = \tilde{\mathbf{A}}\begin{bmatrix} \delta\mathbf{\Omega} \\ \delta\mathbf{q} \end{bmatrix} + \tilde{\mathbf{B}}(t)\mathbf{N}, \tag{4}$$

where $\tilde{\mathbf{A}}$, $\tilde{\mathbf{B}}(t)$ are the system and the control matrices, $\delta\mathbf{\Omega}$, $\delta\mathbf{q}$ are respectively the angular velocity and the attitude deviation from the reference given as the vector part of the attitude quaternion, and $\mathbf{N}$ is the desired control torque. The optimal magnetic moment $\mathbf{m}$ lies on a plane perpendicular to the local geomagnetic field vector, and can be found from:

$$\mathbf{m} = \frac{\mathbf{N} \times \mathbf{B}}{|\mathbf{B}|}, \tag{5}$$

where $\mathbf{B}$ is the local geomagnetic field vector.

The challenge is to find a time invariant counterpart of the system in Eq. (4). This is done by averaging of components of the matrix B(t) over one orbit (see [10]):

$$\tilde{\bar{\mathbf{B}}} = \frac{1}{T_o}\int_o^{T_o} \tilde{\mathbf{B}}(t)dt. \tag{6}$$

Now, standard linear control methods can be applied for the system $(\tilde{\mathbf{A}}, \tilde{\bar{\mathbf{B}}})$. The gain for the science observation controller is computed using linear quadratic optimal (LQ) technique. Weight matrices $\mathbf{Q}_c$, for state, and $\mathbf{R}_c$, for control, have been chosen so that the closed loop time constants of the Ørsted satellite motion are slow compared with the orbital period. In this way the average model in Eq. 6 is not violated. Additional stability analysis for the science observation controller, based on Floquet theory of periodic systems, has been performed in [9].

4.3. Inverted Boom Control

The inverted boom controller is activated when the satellite boom is detected to point towards the Earth. Positions with the boom either up or down are naturally stable equilibria of the satellite motion. The objective of the inverted boom controller is to make the boom upside-down equilibrium unstable. The inverted boom controller is based on an energetic approach developed in [9].

The control gain implemented in the science observation controller is too small to turn the satellite to an upright

position. Therefore, the controller gain is increased by a factor of $k = k_0$, and is kept at this level until the boom is upright. If the boom is detected to be no longer upside-down, the coefficient k is exponentially decreased to $k = 1$. This simple procedure has been proven to be globally stable in [11] and [9].

In addition to theoretical analysis, simulation tests have been carried out. Results for the inverted boom control and the science observation control are depicted in Figures 5 and 6. It is shown that the satellite is retrieved from the upside down equilibrium in plot a) of Figure 5. It is also shown that the satellite trajectory is within the required operational envelope. Difficulties with yaw control are due to the small moment of inertia about the z-principal axis compared with the x- and the y- axes. Minor corrections of pitch and roll introduce a large deviation of yaw. The time history of the factor k is shown in Figure 6, k converges to 1 and the science observation control takes over.

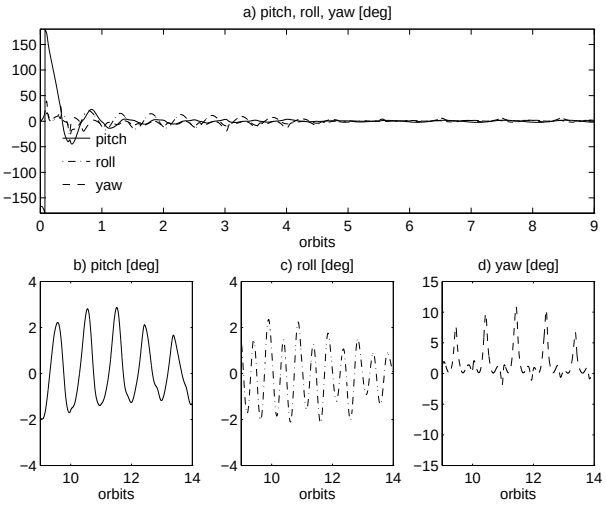

Figure 5: *Simulation of inverted boom and science observation control. After only 4 orbits satellite trajectory is within required operational envelope*.

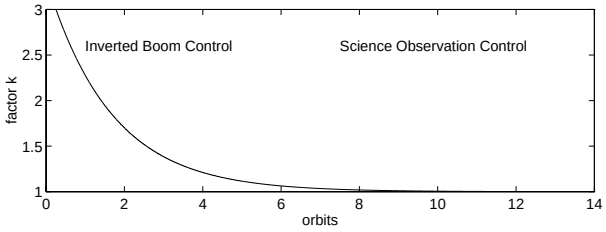

Figure 6: *Factor k converges from $k_0 = 3$ for inverted boom control to* 1 *for science observation control*.

5. ATTITUDE ESTIMATION

After the boom deployment the inertial attitude is available from the star camera with unique accuracy provided its operational conditions are satisfied. This is called *normal* operational mode. In situations with faults or temporary blackout alternative estimates are needed to maintain adequate attitude information for control.

In Ørsted estimates obtained from the star camera are supplemented by a parallel *secondary* attitude estimation algorithm based on the magnetometer and sun sensor. Separating the estimation problem offer several advantages: 1) A second estimate is available for on-board fault detection, 2) a high precision star camera measurement in the Kalman filter would make the transition to sun sensor and magnetometer based estimation difficult in case of camera fault, 3) decreased accuracy of second estimate but overall simplified processing.

The result is an attitude estimation structure as shown in Figure 7.

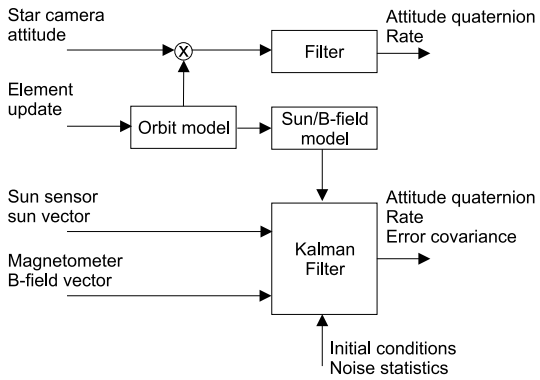

Figure 7: *Attitude estimation conceptual diagram.*

5.1. Normal Operation

The star camera provides an inertial attitude whereas the control system works relative to a local orbit reference. The star camera quaternion therefore has to be composed with an inertial-to-orbit rotation. This rotation is generated by an orbit position model which is dynamically updated from ground approximately every 10th orbit. The rate is estimated from the star camera attitude through composition of the attitude quaternion with its derivative.

5.2. Secondary Operation

Secondary operation is relying on an Extended Kalman Filter (EKF) algorithm primarily based on the magnetic field measurements. Magnetometer measurements offer the advantage of being highly accurate and available at any time, regardless of the mission phase, spacecraft attitude or orbit position. The filter is inherently robust to loss of any single attitude sensor (eg., the sun sensor in

eclipse). Observability with only magnetic field vectors is maintained due to the rotation of the reference vector in orbit (720 deg/orbit) and propagation of the dynamics.

The reference Earth magnetic field is computed as a function of the estimated position based on an 8th-degree spheric harmonic model[1]. A simple Kepler model is used in describing the Earth orbit motion from which the sun vector in the local orbit coordinates is derived as a reference for the Kalman filter.

The filter is implemented as a traditional discrete/continuous filter structure with an alternating state/covariance propagation and measurement update as shown in Figure 8.

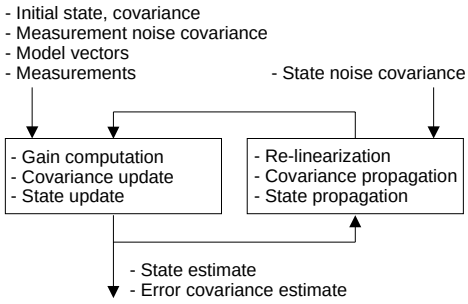

Figure 8: *Kalman filter structure.*

Since the error quaternion corresponds to small rotation, the fourth component δq_4 will be close to unity, and only the three vector components δq are estimated. The filter state becomes

$$\Delta x = [\delta q_1, \delta q_3, \delta q_3, \Delta\omega_1, \Delta\omega_2, \Delta\omega_3]^T . \qquad (7)$$

The body rates are updated by simple addition while the quaternion is updated by multiplication

$$\hat{\omega}_{k^+} = \hat{\omega}_{k^-} + \Delta\hat{\omega}_k \qquad (8)$$

$$\hat{\bar{q}}_{k^+} = \delta\hat{\bar{q}}_{k^+} \otimes \hat{\bar{q}}_{k^-}, \qquad (9)$$

in which $\delta\hat{\bar{q}}_{k^+}$ is the renormalized[2] quaternion.

Between measurement updates the state is propagated based on the equations of motion for the gravity gradient stabilized rigid spacecraft (see [12]).

5.3. Implementation

It is well known that the discrete EKF in its original formulation can be numerically unreliable. The reliability of the EKF has been significant improved by implementing the square-root formulation which provides adequate covariance matrix precision with single precision fixed-point arithmetic. The measurement update is performed using Biermans *Square Root Free* square root observational update, and the covariance time update is based on Thorntons modified weighted Gram-Schmidt orthogonalization [13]. In addition, this process also prevents numerical truncation from generating a covariance matrix that has negative eigenvalues.

5.4. Simulation and Results

A high-fidelity dynamic simulation was developed in order to demonstrate and test the capabilities of the attitude estimation.

The simulated spacecraft model includes sensor misalignment as well as random sensor noise and biases, see [12]. The main error source is due to inaccuracies in the magnetic field model used on-board. To emulate this discrepancy, the Earth magnetic field is simulated using a 10th-degree model, and the on-board model uses a 6th-degree model (real on-board model is of order 8). In general the modeling provide relevant disturbance torques and significant random as well as systematic errors.

To access the expected performance of the filter a simulation was performed with the full order filter. Shown in Figure 9 is the error in attitude, represented by pitch, yaw and roll angles. The attitude determination based on magnetometer and Sun sensor was found effective with accuracies of 0.18-0.25 in pitch/roll, 0.8 deg in yaw and 0.0015 deg/sec in rates, thereby meeting requirements.

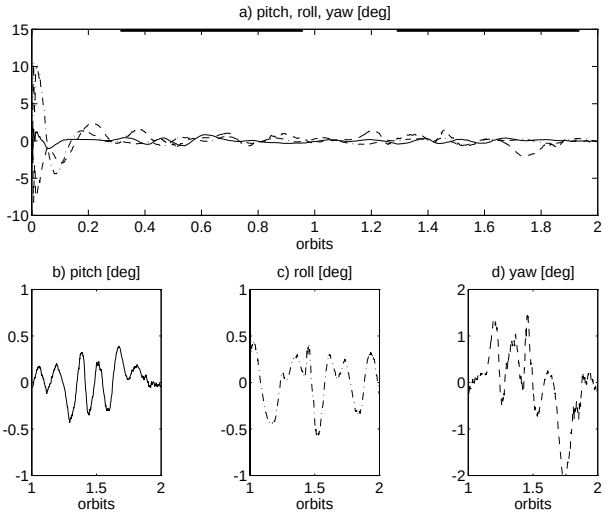

Figure 9: *Simulation of full state filter. Plot a) shows the convergence from a 5 deg initial knowledge error. Plots b)-d) emphasize the converged accuracy. Black bars at the top of a) indicate sun-lit parts of the orbit.*

The initial knowledge error was set to 5 deg and 0.02 deg/sec in all axes. After convergence the accuracy is 0.18 deg, 0.25 deg, and 0.79 deg in pitch, roll and yaw

[1]Coefficients for this mission provided by T. Risbo, Copenhagen University and R.A. Langel NASA Goddard Space Flight Center.

[2]Setting $q_4 = 1$ and dividing the resultant quaternion components by the square root of the sum of their squares.

(1 RMS). The yaw motion is clearly the most difficult to estimate which is due to the lowest inertia about the spacecraft yaw (boom) axis. The errors in rate knowledge are below 0.0015 deg/sec for all three components of the angular velocity.

Neither the magnetic field model discrepancies nor the Sun sensor errors are white Gaussian sequences as assumed in the modeling. Neglected are also variations in the orbital rate due to the orbit eccentricity and aerodynamic drag. They all contribute to non-white systematic errors.

5.5. Convergence From Large Initial Errors

The ability of the filter to converge from large initial attitude knowledge errors was investigated. The initial knowledge error are set to 45 deg in all axes and the rate error are set to 0.01 deg/sec. The result is shown in Figure 10. Within one orbit the filter clearly meet requirements.

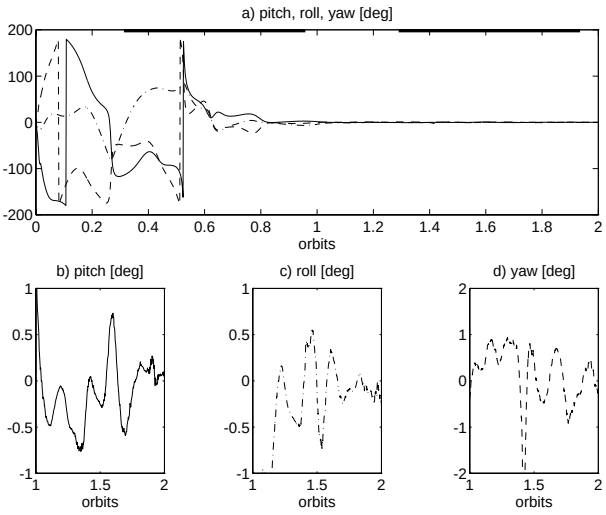

Figure 10: *Filter convergence from a 45 deg initial attitude error*.

6. SUPERVISORY CONTROL

The supervisor shall monitor attitude estimation and control hardware for faults, handle changes between operational phases, and provide interface for commands and telemetry as seen in the three-layer structure, Figure 2. The Ørsted supervisor is designed and implemented in a structural manner with the aim to increase overall reliability of the entire system. The supervisory algorithm constitute itself an increased risk for failures (in the software), so the overall reliability is only improved if the supervisory level is absolutely trustworthy.

This chapter describes the design procedure which involves a broad range of aspects. Only the very important problem of fault coverage will be studied in detail in this paper. It is crucial, that the supervisor implementation agrees with the design requirements, and a method to support this is introduced.

6.1. Supervisor Design Procedure

The rules of the supervisor are designed and checked using the design procedure shown in Figure 11. A short summary of the design steps follows below, and a detailed description can be found in [14].

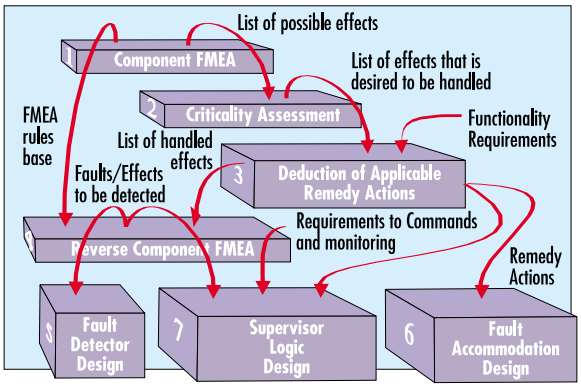

Figure 11: *Systematic supervisor design approach. These seven actions conduct the designer from an analysis of failures to the design of fault detectors, supervisor logic, and fault accommodation.*.

1. A Failure Mode and Effects Analysis (FMEA) of all involved sub-systems (magnetorquer power drives, star camera, sun sensors, CSC magnetometer, etc.) is performed and combined into a complete analysis of the entire satellite. The end-effects describes consequences on top level (eg. satellite tumbling, control error increases, etc.). The FMEA technique used in this context is described in [15].

2. The top level end-effects are judged for severity, and the ones with significant influence on the control performance are selected to be handled by the supervisor.

3. The possibilities of fault accommodation are considered. This includes enabling and disabling of redundant units (magnetorquers, power drives, and sun sensors), selection between the two attitude estimation algorithms (normal and secondary operational mode), and otherwise graceful degradation and close down. The point of reconfiguration determines the requirements for fault isolation. It is not necessary to isolate faults below the level where the fault effect propagation can be stopped.

4. A reverse deduction of the FMEA rule base is performed to locate the faults that cause the considered end-effects. The deduction is performed down to the point of reconfiguration as determined in step 3.

5. Fault detector algorithms are designed. Most fault events are detected by simple means like range and rate check on sensor signals, but also the magnetic coupling from the magnetorquers to the magnetometer is exploited to catch anomalies in the power drives and magnetorquers. Isolation of sun sensor faults uses innovations from the extended Kalman filter used in secondary attitude estimation.

6. Fault accommodation actions are designed. The Ørsted supervisor involves only simple selection of control level algorithms, enabling and disabling of redundant hardware, and activation/deactivation of the entire controller.

7. Supervisor inference rules are designed using the information about which faults/effects are detected and how they are accommodated. The supervisor determines the most appropriate action from the present condition and commands.

These steps are followed to make the supervisor design cheaper, faster, and better. The fault coverage is then (hopefully) as complete as possible, because the FMEA step includes in principle all possible faults. The analysis is modular, because small sub-systems are treated individually. Furthermore, the strategy has the advantage that the system is analyzed on a *logical* level as far as possible before the laborious job of mathematical modeling and design is initiated. This ensures that superfluous analysis and design are avoided.

6.2. Consistent and Complete Supervisor

The attitude control system for a small satellite like Ørsted would immediately seem rather uncomplicated, but there may be interconnections between sub-systems which in the run-time system causes the supervisor to deviate from the design aims. An obvious innocent cross correlation may be neglected and show up to be significant. This section illustrates how a computer toolbox for boolean logic processing is used to prove correctness.

The supervisor rules designed in step 7 (see above) are implemented in the Beologic Array Inference Toolbox (AIT), see [16]. This is a commercial product from Bang & Olufsen (Denmark) that supports the analysis of logical networks. AIT is used during the design phase to make a completeness check of the supervisor logic for fault handling to verify that the fault accommodation actually stops the propagation of faults, and that it is consistent with the design requirements. This is done by implementing rules for the complete logical data flow of the reconfigurable system as illustrated in Figure 12.

The figure shows the logical data flow of fault propagation (true or false) from sub system FMEA to top level consequences as end-effects. The rules of the fault detectors simply states (true or false) that a certain fault effect

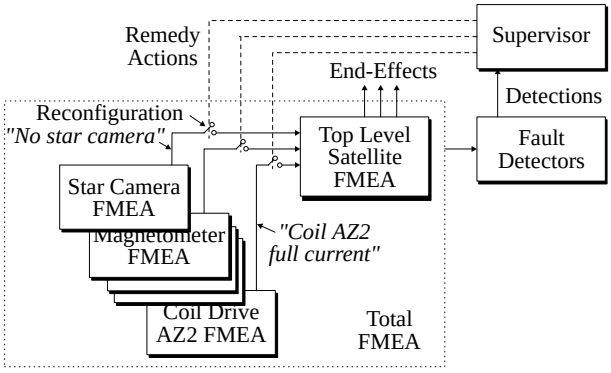

Figure 12: *The principle of fault detection and reconfiguration. A fault that occurs in some sub-system will propagate through the system, be identified by a detector, and the supervisor reconfiguration will stop the fault propagation.*

can be detected or not. The supervisor represents the exact run-time rules that use the boolean fault detections to determine remedy actions. These actions are now written in AIT as rules that disable the propagation of faults, as it would do in the real implementation. In a logical sense, the termination of fault propagation means that the fault effect is no longer active and hence the corresponding detection will be false. This fact constrains the faults that are successfully accommodated to be forced in-active. If they were true there would be a contradiction in the rule base. A very powerful completeness check of the supervisor rules is based on this *logical feedback*. The rule base is automatically checked and a list of faults bound to false is generated. The list is examined to verify that all the faults expected to be accommodated actually are handled by the supervisor rules.

6.3. Example on Supervisor Completeness Check

A simple example on the check for supervisor rule base completeness is the star camera (SIM) black out handling.

The propagation of a black out (`SIMFault=true`) is given by the rule:

```
SIMFault_ = (AD_OP_NO and SIMFault)
```

which states that the SIM fault will have the effect `SIMFault_=true` when the SIM is used for attitude determination (`AD_OP_NO=true`). The SIM fault will propagate through the top level FMEA and cause the satellite to experience a random tumbling motion:

```
RandomMotion = ((Phase_Normal and
(ADUncertHigh_ or SSA1Low_ or SSB1Low_ or SIMFault_))
or CSCFault_ or CD2MMax_ or CD3MPos_)
```

In this rule, numerous other causes for the same end-effect are included, but these are not essential in this con-

text. It should be noticed, anyhow, that the SIM fault only causes an effect when the satellite is in the science observation phase, where the boom is out (`Phase_Normal=true`). A SIM fault is easily detected because the star camera will stop the generation of data. Hence, the detector rule simply states that a SIM fault is detected:

```
DET_Sim_Fault = SIMFault_
```

When a SIM fault is detected the supervisor will disable SIM based attitude estimation (`AD_OP_NO=true`) and switch to the backup algorithm using sun sensors and magnetometer instead (`AD_OP_NO=false`):

```
(Phase_Normal and !DET_Sim_Fault) = AD_OP_NO
```

It is easy for this small rule base to see that the variable `SIMFault_` *cannot* be true and the supervisor reconfiguration is thus confirmed. The entire Ørsted supervisor rule base is much more complicated so it is advantageous to use a computer tool to support this verification.

6.4. Fault Scenario

Numerous simulations have verified performance during a wide range of fault conditions. As an example, combined attitude control and estimation results are shown in Figure 13 for a situation with star camera blackout. The attitude errors are referred to the nominal attitude.

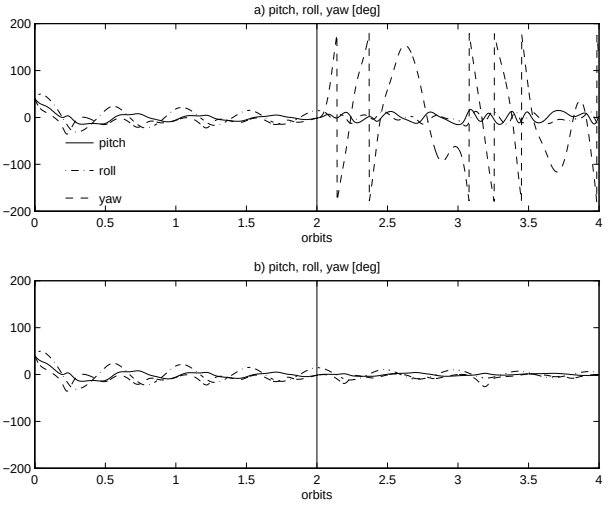

Figure 13: *Simulated attitude determination and control. Star camera blackout after 2 orbits. In plot a) no reconfiguration is performed. In b) the attitude determination is reconfigured.*

The initial attitude is 40 deg in all three angles and the star camera is simulated to black out after two orbits. The two simulations clearly show the necessity to reconfigure attitude acquisition to be based on sun sensors and magnetometer instead of the star camera. If no reconfiguration takes place, the satellite will begin rotating about the boom axis.

7. CONCLUSION

The paper has presented some new approaches to design and implementation of attitude control systems for small satellites that increase the level of autonomy. The entire ACS was divided into attitude estimation, attitude control, and supervisory control, such that each item could be designed and tested separately.

A structural approach to the supervisor control level was introduced that improves completeness and consistency of the supervisor and improves overall fault tolerance. A toolbox for logical processing was presented that is able to automate some of the troublesome tasks in the development of large rule bases.

A gyro-less attitude determination system with two algorithms operating in parallel was presented. The primary system, based on a star camera, was supplemented with a Kalman filter, using sun sensor and magnetometer data. In case of star camera black out, the backup algorithm is enabled, introducing a significant degree of autonomy.

Attitude control principles were presented for all operational situations: Initial detumbling after ejection from the launcher, three-axis stabilization in normal operational mode, and inverted boom control for acquiring the nominal attitude. Simulations show that three-axis stabilization is possible with magnetic actuation only.

ACKNOWLEDGMENTS

This work was supported by the Ørsted satellite project.

REFERENCES

1. ESA Sep. 1996, Ulysses spacecraft home page, $http://helio.estec.esa.nl/ulysses/spacecraft.html$, Published on Internet.

2. Eliason, E. Oct. 1994, Clementine information home page, $http://nssdc.gsfc.nasa.gov/planetary/cleminfo.html$, Published on Internet.

3. Day, R. M. and M. Bay Jun. 1996, Xte: Astronomy with autonomy, *Aerospace America*, pp. 34–39.

4. Lisman, S. S. Jun. 1996, Autonomous guidance and control, new millennium presentation, $http://nmp.jpl.nasa.gov/events/workshop/proceedings/workshop.html$, Workshop presentation accesible on Internet.

5. Nakatani, I. Jul. 1996, Autonomous systems for planetary missions, Lecture notes, ISU summer session, Vienna, Austria, Institute of Space and Astronomical Science.

6. Nielsen, O.V., B. Hernando, J.R. Petersen and F. Primdahl 1990, Miniaturisation of low-cost

metalic glass flux-gate sensors, *Magnetism and Magnetic Materials*, 83, 404–406.

7. Jørgensen, J.L., A. Eisenmann, C.C. Liebe and G.B. Jensen Nov. 1996, The advanced stellar compass onboard the ørsted satellite, in *3rd ESA International Conference on Spacecraft Guidance, Navigation and Control Systems*.

8. Wisniewski, R. Nov. 1994, Attitude control methods, Tech. Rep. Ørsted Project TN-232, Aalborg University.

9. Wisniewski, R. Feb. 1997, *Satellite Attitude Control with Use of Magnetic Coils Only*, Ph.D. thesis, Aalborg University, Denmark.

10. Martel, F., K.P. Parimal and M. Psiaki September 1988, Active magnetic control system for gravity gradient stabilized spacecraft, in *Annual AIAA/Utah State University Conference on Small Satellites*.

11. Wisniewski, R. and M. Blanke Jun. 1996, Three-axis satellite attitude control based on magnetic torquing, in *13th IFAC World Congress, San Francisco, California*.

12. Bak, T. Nov. 1996, Onboard attitude estimation for a small satellite, in B H Kaldeich-Schurmann, editor, *3rd ESA International Conference on Spacecraft Guidance, Navigation and Control Systems*. European Space Agency.

13. Grewal, M. S. and A. P. Andrews 1993, *Kalman Filtering, Theory and Practice*, Information and System Science Series, Prentice Hall.

14. Bøgh, S. A., R.I. Zamanabadi and M. Blanke Oct. 1995, On-board supervisor for the ørsted satellite attitude control system, in *Artificial Intelligence and Knowledge Based Systems for Space*, pp. 137–52. ESA-ESTEC.

15. Blanke, M., R. B. Jørgensen and M. Svavarsson 1995, A new approach to design of dependable control systems, in *KoREMA Workshop, Zagreb, Croatia*.

16. B&O, Bang & Olufsen 1996, *Array Inference Toolbox, User's Manual, Personal Computers*, Denmark.